

Dalton Transactions

An international journal of inorganic chemistry

Accepted Manuscript

This article can be cited before page numbers have been issued, to do this please use: P. Arosio, F. Orsini, F. Brero, M. Mariani, C. Innocenti, C. Sangregorio and A. Lascialfari, *Dalton Trans.*, 2023, DOI: 10.1039/D2DT03387A.



This is an Accepted Manuscript, which has been through the Royal Society of Chemistry peer review process and has been accepted for publication.

Accepted Manuscripts are published online shortly after acceptance, before technical editing, formatting and proof reading. Using this free service, authors can make their results available to the community, in citable form, before we publish the edited article. We will replace this Accepted Manuscript with the edited and formatted Advance Article as soon as it is available.

You can find more information about Accepted Manuscripts in the [Information for Authors](#).

Please note that technical editing may introduce minor changes to the text and/or graphics, which may alter content. The journal's standard [Terms & Conditions](#) and the [Ethical guidelines](#) still apply. In no event shall the Royal Society of Chemistry be held responsible for any errors or omissions in this Accepted Manuscript or any consequences arising from the use of any information it contains.

PERSPECTIVE

The effect of size, shape, coating and functionalization on nuclear relaxation properties in iron oxides core-shell nanoparticles: a brief stock of the situationPaolo Arosio,^{*a} Francesco Orsini,^a Francesca Brero,^b Manuel Mariani,^b Claudia Innocenti,^c Claudio Sangregorio^c and Alessandro Lascialfari^bReceived 00th January 20xx,
Accepted 00th January 20xx

DOI: 10.1039/x0xx00000x

In this perspective we present a short selection of some of the most significant case studies of magnetic nanoparticles for potential applications in nanomedicine, mainly Magnetic Resonance. For almost 10 years, our research activity focused on the comprehension of the physical mechanisms at the basis of the nuclear relaxation of magnetic nanoparticles in the presence of magnetic fields; taking advantage of the insights gathered over this time span, we report on the dependence of relaxation behaviour on the chemico-physical properties of the magnetic nanoparticles and discuss them in full details. In particular, a critical review is carried out on the correlations between their efficiency as contrast agents in Magnetic Resonance Imaging and the magnetic core of magnetic nanoparticles (mainly iron oxides), their size and shape, as well as the coating and solvent used for making them biocompatible and well dispersible in physiological medium. Finally, the heuristic model proposed by Roch and coworkers is presented, as it was extensively adopted to describe most of experimental data sets. The large amount of data analyzed allowed us to highlight both advantages and limits of the model.

1. Introduction

In the last decades, the interest of several multidisciplinary research groups has been attracted towards magnetic nanoparticles (MNPs) for the unique properties arising from their size scale. Among the various areas in which they are employed, MNPs have been found to be promising systems for several biomedical applications¹⁻⁴. Besides their traditional use as contrast agents in Magnetic Resonance Imaging (MRI)⁵⁻¹¹ and in other multimodal techniques,¹²⁻¹⁸ their implementation as therapeutic agents in Magnetic Fluid Hyperthermia (MFH),¹⁹⁻²⁴ nanovectors for local drug delivery,^{6, 25-30} cell separation and biosensing applications,³¹⁻³⁶ were extensively studied.

MNPs proposed for biomedical use typically consist of a magnetic core of transition metals oxides (iron, cobalt, nickel, manganese, etc.) coated with a shell of organic moieties like e. g. polymers, sugars, acids, and dispersed in water or physiological media. For biomedical applications, engineering of the surface appears to be a crucial step in order to obtain

colloidal stability, biocompatibility and biodegradability^{4, 22, 27, 28, 37, 38} as well as to mitigate their nonspecific uptake by the reticuloendothelial system.³⁹ Thanks to the "intrinsic" biocompatibility of iron, the most widely investigated MNPs are composed of a magnetite (Fe₃O₄) or maghemite (γ -Fe₂O₃) core, i.e. ferrimagnetic materials that behave as a single domain at the nanoscale (below about 150 nm), with superparamagnetic behaviour and consequently zero remanent magnetization due to thermal fluctuation. Magnetite and/or maghemite MNPs are preferred over other iron oxides for their high magnetic moment and their strongly reduced possibility to agglomerate once removed the applied magnetic field.

For medical applications it is also fundamental to focus on and study the possible adverse effects of nanoparticles on human health. Charge and surface coating of iron oxides MNPs definitely influence their interaction with human body.⁴⁰ In the past, it was demonstrated that bare and coated (with -NH₂ and -COOH) small iron oxides MNPs induced different responses depending on the specific cell lines of brain, heart and kidneys.⁴¹ On the other hand, also the routinely used coatings, as dextran, polyethylene oxide, citric acid, etc., must be tested accurately for every new MNPs proposed, to assure that no toxic moieties overcome the coating layer. Also nanoparticles coated with polyethylene glycol (PEG), that is known to reduce the immunological response, could be more toxic than the same MNPs covered with other coatings.⁴² Different kind of toxicity should be also taken into account. Recently, we studied the effect of iron oxides MNPs coated with meso-2,3-dimercaptosuccinic acid on cell proliferation of pancreatic cancer cells showing how the commonly used Trypan Blue assay

^a Dipartimento di Fisica, INFN and INSTM RU, Università degli Studi di Milano, 20133 Milano, Italy.

^b Dipartimento di Fisica, INFN and INSTM RU, Università degli Studi di Pavia, 27100 Pavia, Italy.

^c Dipartimento di Chimica, Università di Firenze and INSTM, 50019 Sesto Fiorentino (FI), Italy; ICCOM-CNR, 50019 Sesto Fiorentino (FI), Italy.

† Corresponding author P.A. orcid.org/0000-0003-2388-0402, email: paolo.arosio@unimi.it; Orcid numbers of other authors: F.O. orcid.org/0000-0001-5601-9825, F.B. orcid.org/0000-0003-1822-8217, M.M. orcid.org/0000-0001-8516-9662, C.I. orcid.org/0000-0003-3705-4283, C.S. orcid.org/0000-0002-2655-3901, A.L. orcid.org/0000-0002-1687-0436.

Electronic Supplementary Information (ESI) available: [details of any supplementary information available should be included here]. See DOI: 10.1039/x0xx00000x



reveals a poor toxicity of MNPs, while the clonogenic survival studies quantified a toxicity around 50–60%.⁴³

The above quoted papers are examples of toxicology studies on iron oxides-based MNPs that show how the lack of knowledge about the mechanisms involved in their possible toxicity implies a big work of specific characterization whenever a new product is proposed for MNPs implementation in nanomedicine.

Although a considerable number of different MNPs have been developed for biomedical applications, a full understanding of the physical mechanisms that occur in the presence of biological media and their relationship with the characteristics of the MNPs – such as core composition, size, shape, coating, dispersant, and functionalization – has not been achieved yet.

To date, Gadolinium-based molecules are the most common contrast agents used for MRI. The main reasons are: (i) the possible use of extravascular^{44,45} and intravascular gadolinium chelates⁴⁶; (ii) the higher accuracy of Gd-based-Enhanced MR Angiography compared with that of conventional contrast angiography; (iii) the ability to cross the blood–brain barrier.

As concerns the MNPs, the complex parameters influencing contrast enhancement make their development as non-specific CA unsuitable. Nevertheless, their unique features, related for instance to the surface functionalization, may address the research efforts toward the realization of target-specific CAs.

Superparamagnetic iron oxide MNPs could be used as MRI contrast agents (CAs), as already done in the past for some approved materials (e.g. Endorem) and later retrieved from the market for commercial reasons, because they increase the nuclear relaxation rates, (mainly the transverse one,^{47,48}) of the ¹H nuclei contained in the human body. The nuclear relaxivities are defined as

$$r_i = \left(\frac{1}{T_{i, meas}} - \frac{1}{T_{i, dia}} \right) / C \quad (1)$$

where $i = 1, 2$ are respectively referred to the nuclear longitudinal relaxation time T_1 and the nuclear transverse relaxation time T_2 . $1/T_{i, meas}$ is the nuclear relaxation rate measured on a sample dispersion, $1/T_{i, dia}$ the nuclear relaxation rate of the diamagnetic host solution and C the concentration of the magnetic center in $\text{mmol} \cdot \text{l}^{-1}$.

The physical mechanisms involved in the change of nuclear relaxation rates induced by MNPs are the subject of many current researches aiming at developing new models to direct the design of optimal MNPs.^{31, 49–53} The spin dynamics and the MNP nuclear relaxation behavior critically depend on the intrinsic properties of the MNPs (size, core type, etc.) as well as on the intensity of the external applied magnetic field, the temperature of application and the solvent used to disperse MNPs, as reported in Figure 1.

In the case of functionalized MNPs, the coating plays a crucial role. The ideal one should consist in organic compounds which would be able to both affect the water molecules diffusion, causing a variation of nuclear relaxivity, and allows fast exchange to allocate the maximum number of water molecules near CAs. Nowadays, there is an extensive use of PEG chains

which increase transverse relaxivity, due to the slowing down of the diffusion, while hydrophobic polymers decrease r_2 values.⁵⁴

Moreover, other different functionalization can affect the correlation times (mainly the exchange of protons between the particle surface and bulk water, the free water molecules translation, diffusion, and rotation with respect to the MNP) which then lead the nuclear relaxation.

For single domain MNPs, where all the atoms coherently respond to the external magnetic field,^{55–57} a magnetic moment, given by the sum of the spins inside the particle (as the orbital part is generally quenched for 3d metals), is associated to particle. A uniaxial magnetic anisotropy energy, characterized by two minima,^{4, 58, 59} is invoked to model the magnetization reversal, the typical time scale of which is the Néel relaxation time (τ_N). Other characteristic correlation times are the Brownian time (τ_B) and the diffusion time (τ_D), both related to the MNPs motion, and, wherever present, the so-called chemical exchange time (τ_{ex}), related to the exchange process between a water molecule coordinated to the MNP surface and a water molecule of the medium.

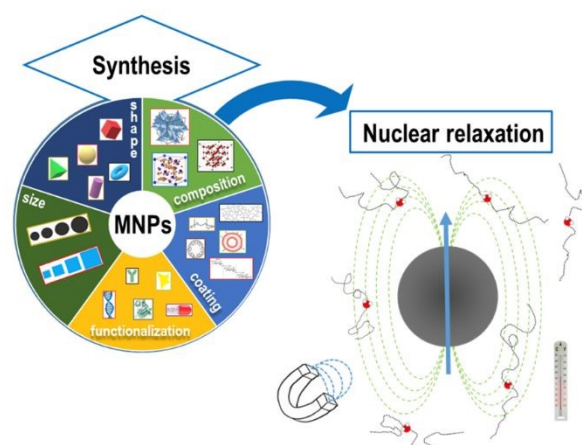


Figure 1. Schematic representation of the principal intrinsic parameters, on the left (magnetic core composition, size, shape, coating, surface functionalization) and extrinsic parameters, on the right (solvent, magnetic field, temperature) relevant for describing the MNP nuclear relaxation process.

In this perspective, we present the results obtained studying a quite large number of superparamagnetic MNPs which differ in core size, core composition, shape, surface coating material and solvents used to obtain colloidal solutions. This roundup of studies offers the opportunity: 1) to discuss the obtained experimental evidences, 2) to test the efficacy of the Roch heuristic model on many different materials for describing the superparamagnetic MNPs relaxation, 3) to present some possible future perspectives in this research field.

It should be noticed that, the well-known model developed by Roch et al [60] was commonly used to fit the NMR dispersion (NMR-D) profiles. Indeed, an evaluation of important parameters such as the relaxation times, the distance of minimum approach of water molecules to MNPs, r_d , the saturation magnetization, M_s , and the magnetic anisotropy



energy barrier, E_A , can be obtained by fitting the longitudinal NMR dispersion curves.

After a first section dedicated to the synthesis and characterization methods, we present the theoretical background useful to describe the influence of the magnetic core intrinsic properties (composition, size and shape) on the relaxation properties. In the next section, we discuss the impact of changing the solvent of the colloidal solutions and the role of the surface coating and its functionalization. In the last section, some general comments on the whole set of results obtained in these 10 years of research and some perspectives are proposed.

2. Synthetic procedures and characterization methods

For a detailed description of the synthetic procedures and experimental characterizations of the different MNPs, the readers are suggested to refer to the corresponding articles. In this section, only the most relevant hints on the synthesis methods and the principal chemico-physical characteristics are reported.

In ref. 61 four series of ferrite-based MNPs with core size between 4 and 20 nm were obtained by thermal decomposition method starting from different metal-organic precursors. The studied MNPs were: rhamnose-coated magnetite MNPs (S - Mag), oleate coated magnetite particles (P - Mag), oleic acid-coated manganese ferrite nanocrystals (MnFe) and non-stoichiometric oleic acid-coated cobalt ferrite MNPs (CoFe). In the case of the two series of magnetite MNPs, once properly coated, the samples were dispersed in water solutions.

In ref. 62, γ -Fe₂O₃ MNPs coated with oleic acid were again synthesized by thermal decomposition and transferred in water after the substitution of oleic acid with polyacrylic acid. Three samples of MNPs of magnetic cores size of 10, 14 and 19 nm were studied.

A systematic investigation of $\text{Co}_x\text{Zn}_y\text{Fe}_{3-(x+y)}\text{O}_4$ MNPs synthesized by thermal decomposition with, on average, 8 – 9 nm size was reported in 63, where the amount of cobalt was kept constant at ca. $x = 0.6$, while the Zn amount was varied in the range $0 < y < 0.4$.

According to surfactant mediated colloidal routes in high boiling organic solvents under nitrogen atmosphere, iron oxide based MNPs were prepared in 64 with different core size, morphology and dispersing media. In details, three core sizes (mean diameter $d = 3, 8$ and 17 nm) of spherical samples dispersed in an organic non - polar solvent (hexane) were prepared. In addition, 8nm spherical sample suspended in water (without removing the ligand directly attached at the surface of the inorganic core) and cubic shaped sample dispersed in hexane with the same volume of the 8nm spherical MNP were also prepared.

Aqueous dispersions of two series of maghemite MNPs of different mean diameters ($d = 17$ and 8 nm) coated with four different types of biocompatible negative polyelectrolytes, synthesized by adding each polyelectrolyte to an acidic solution

of MNPs and, after dialysis against water, alkalizing the solutions with hydroxide ammonium were studied in 65.

Lastly, functionalized coating MNPs were investigated in 66 and 67; ref. 66 regarded magnetite MNPs coated with random multiblock poly(ester - ether - urethane)s copolymers (PEEU) of PCL and PEG decorated with folate and loaded with paclitaxel (PTX), designed to target the human breast MDA-MB-231 tumor. Ref. 67 was focused on the use of synthetic polyamide mimics of natural DNA and RNA, the Peptide Nucleic Acid (PNA) oligomers, for the functionalization of iron oxide nanoparticles with magnetic core dimension of 17 nm, in order to obtain a water soluble hybrid nanomaterial.

The chemical - physical characterization for all the studied MNPs was based on elemental analysis, X-ray diffraction, Transmission Electron Microscopy, Dynamic Light Scattering and, where possible, Atomic Force Microscopy.

For the magnetic properties measurements, DC magnetization and AC magnetic susceptibility were recorded on dry powder samples or concentrated colloidal solutions by Superconducting Quantum Interference Device (SQUID) magnetometers. The hysteresis curves were collected as a function of the magnetic field (up to ± 5 T) at different temperatures (300 K and 5 K). Zero-Field-Cooled (ZFC) and Field-Cooled (FC) magnetization curves were recorded as a function of temperature (5 - 300 K) at different static magnetic fields (ranging from 0.005 to 0.3 T) after cooling samples in the absence (ZFC) or in the presence (FC) of the measuring field. AC magnetic susceptibility data were collected as a function of temperature (5 - 300 K) in the frequency range 1 - 1000 Hz.

The local spin dynamics and the MRI contrast efficiency were assessed by means of ¹H nuclear magnetic resonance (NMR) relaxometric characterization. The NMR - dispersion profiles were collected at room temperature by measuring the longitudinal (T_1) and the transverse (T_2) nuclear relaxation varying the Larmor frequency of the investigated nuclei ($2\pi\nu_L = \gamma B_0$, where $\gamma = 2.67513 \cdot 10^8 \text{ rad s}^{-1} \text{ T}^{-1}$ is the gyromagnetic factor of ¹H) from 10 kHz up to 60 MHz and only for one case up to 120 MHz.⁵⁶ For low-frequency relaxation measurements (from 0.01 MHz to 5.0 MHz), the Fast-Field-Cycling technique was used by using a Smartracer Stellar NMR relaxometer. Higher-frequency ($\nu_L > 5.0\text{MHz}$) relaxation measurements were performed using a Stellar Spinmaster and an Apollo - Tecmag Fourier Transform nuclear magnetic resonance (FT-NMR) spectrometers. For $\nu_L < 5.0$ MHz, pre - polarized Saturation Recovery (for T_1) and spin - echo (for T_2) sequences were adopted. For frequencies $\nu_L > 5.0\text{MHz}$, non-pre - polarized Saturation Recovery (SR) and Carr Purcell Meiboom Gill (CPMG) pulse sequences were used for T_1 and T_2 measurements, respectively.

3. Results

3.1 Theoretical background

In order to understand the nuclear magnetic relaxation behaviour of superparamagnetic MNPs and therefore predict their efficiency as CAs in MRI, many models have been proposed in the literature.^{58, 60, 68 - 70} Many of these models assume that



the dipolar magnetic field of the superparamagnetic MNPs produces local magnetic inhomogeneity which in turn modify the nuclear relaxation processes of the dispersant protons with respect to the ones in the pure solvent. Essentially, the nuclear relaxation depends on the fluctuating hyperfine interaction between the high magnetic moment of the superparamagnetic MNPs and the nuclear magnetic moment of the hydrogen nuclei of the solvent. Indeed each proton experiences magnetic fluctuations because of its free diffusion in the magnetic inhomogeneity and the relaxation of the superparamagnetic MNPs magnetization due to the Néel and Brownian processes. The importance of the role played by the superparamagnetic MNP size and composition can be highlighted by considering the simplest case of uniaxial anisotropy, where the anisotropy energy per nanoparticle, E_A , is correlated to its volume, V , and its anisotropy constant, K , which depends on the MNP composition, according to:

$$E_A = K \cdot V \cdot \sin^2 \theta \quad (2)$$

where θ is the angle between the magnetic moment vector and the anisotropy axis (easy axis). Following eq. (2), the two energy minima ($\theta = 0, \pi$), separated by the energy barrier E_A , correspond to the orientation of the MNP magnetic moment along the easy axis and the characteristic time for overcoming E_A , relaxing toward a steady state in the absence of external magnetic field, is the so called Néel relaxation time,⁷¹ which for non-interacting nanoparticles is given by:

$$\tau_N = \tau_0 e^{\frac{E_A}{k_B T}} \quad (3)$$

In eq. (3) the Néel relaxation time depends exponentially on the ratio between anisotropy (E_A) and thermal energy ($k_B T$) and, linearly, by a prefactor, τ_0 , that is of the order of 10^{-9} s for non-interacting MNPs.

When MNPs interact each other, eq. (3) must be modified to correctly describe the experimental results. According to the Vogel - Fulcher model [72], a phenomenological parameter, T_0 , whose value is proportional to the inter-particle interaction, is introduced and the eq. (3) becomes

$$\tau_N = \tau_0 e^{\frac{E_A}{k_B(T-T_0)}} \quad (4)$$

For biomedical applications, MNPs are normally dispersed in liquid, where they can randomly rotate and collide with solvent molecules (Brownian motion), thus inducing the magnetization relaxation with the characteristic Brown relaxation time:

$$\tau_B = \frac{3\eta V_H}{k_B T} \quad (5)$$

where η is the viscosity of the liquid and V_H the hydrodynamic volume of the particle. The Brownian relaxation is more efficient than Néel process for MNPs with high magnetic anisotropy and/or high external magnetic field. In this case, indeed, the superparamagnetic MNPs magnetic moment,

anchored to the crystalline lattice by the high anisotropy energy, tends to be oriented along the external magnetic field through the rotation of the whole particle. It is worth noting that the Brownian relaxation is poorly effective when superparamagnetic MNPs are embedded into the tissues where the rotation of the entire nanoparticle may be partially hampered. Taking into account generic environmental conditions, an effective relaxation time, τ , is thus commonly introduced for weighing the two relaxation processes:

$$\frac{1}{\tau} = \frac{1}{\tau_N} + \frac{1}{\tau_B} \quad (6)$$

In order to deeply investigate the physical mechanisms at the basis of the nuclear relaxation of superparamagnetic MNPs, ¹H-NMRD profiles, *i.e.* the nuclear relaxivities r_1 and r_2 vs frequency for constant T, must be collected in the widest possible frequency range (or, equivalently, the widest applied magnetic field range), possibly including the frequencies associated to the fields used in the clinical practice.

As already stated in the introduction, the analysis of the ¹H - NMRD profiles allows the estimation of some fundamental physical quantities of the MNPs, such as the Néel correlation time τ_N , felt by NMR, the distance of minimum approach r_d of water molecules to MNPs and the magnetic anisotropy. To this aim the experimental ¹H - NMRD profiles, obtained measuring the MNPs samples here reported, were interpreted by using the heuristic model of Roch *et al.*,⁶⁰ where the expressions for the relaxivities, r_1 (eq.(7)) and r_2 (eq.(8)), employed in our work to perform the fitting procedure, are obtained by a linear combination of two contributions describing the high and low magnetic anisotropy cases, respectively:

$$r_1 = \frac{32\pi}{135000} \mu_{sp}^* \gamma_I^2 \left(\frac{N_a c}{r_d D}\right) x \left\{ 7P \frac{L(x)}{x} J^F(\omega_s, \tau_D, \tau_N) + \left[7Q \frac{L(x)}{x} + 3(P+Q)(1-L^2(x) \mp 2\frac{L(x)}{x}) \right] x J^F(\omega_I, \tau_D, \tau_N) \right\} \quad (7)$$

$$r_2 = \frac{16\pi}{135000} \mu_{sp}^* \gamma_I^2 \left(\frac{N_a c}{r_d D}\right) x \left\{ 13P \frac{L(x)}{x} J^F(\omega_s, \tau_D, \tau_N) + 7Q \frac{L(x)}{x} J^F(\omega_I, \tau_D, \tau_N) + 6Q \frac{L(x)}{x} J^F(0, \tau_D, \tau_N) + (1-L^2(x)) \right\} \quad (8)$$

where μ_{sp}^* is the effective magnetic moment locally felt by the protons, γ_I the proton gyromagnetic ratio, N_a Avogadro's number, c the molar concentration of magnetic part of the nanoparticles, r_d the minimum approach distance between protons and superparamagnetic MNPs, D the self-diffusion coefficient of the medium, $L(x)$ the Langevin's function (where $x = \mu_{sp}^* B_0 / k_B T$), $\tau_D = (r_d)^2 / D$ the diffusion time that characterizes the fluctuation of the hyperfine interaction among the nuclear magnetic moments of the solvent ¹H nuclei and the superparamagnetic MNPs magnetic moment, τ_N the Néel relaxation time at room temperature, ω_s and ω_I the electron and proton Larmor frequencies, respectively. The



parameters P and Q are related to the degree of magnetic anisotropy of the system, being the weight of the spectral density functions J^A and J^F , respectively ($P = 0$ and $Q = 1$ for highly anisotropic systems, i.e. $E_A \rightarrow \infty$, while $P = 1$ and $Q = 0$ for low anisotropic systems, i.e. $E_A \rightarrow 0$, and $P + Q \leq 1$). Consequently, for materials with increasing magnetic anisotropy energy and/or increasing the size of the magnetic cores, Q would progressively increase toward 1.

In order to reduce the number of the free parameters of the model, wherever possible, some quantities, independently evaluated with other experimental techniques, were used. For instance, the effective magnetic moment μ_{sp}^* can be estimated by the saturation magnetization value, M_s , obtained through magnetometry techniques, and by the average volume of the particles. In addition, TEM and AFM data can be used to establish reasonable constraints for the distance of minimum approach, r_d , as it is expected to vary between the core diameter (TEM estimate) and the whole size of superparamagnetic MNPs, which includes the coating layer (AFM estimate).

3.2 The role of the magnetic core

The first example of the *modus operandi* explained at the end of the previous paragraph was proposed in 61, where longitudinal relaxivities r_1 curves were acquired experimentally on four different sets of MNPs dispersed in toluene or in ultrapure water. The use of the fitting model allowed us to investigate the dependence of Néel and Curie contributions to nuclear relaxation on magnetic core diameter and ion species and consequently the correlated dependence on magnetic anisotropy energy density. In this study the obtained distances of minimum approach of the solvent molecules to the magnetic centres suggested the impossibility of the solvent to completely penetrate the organic coating. A notable comparison between the Néel relaxation time for all the samples obtained by the fitting of NMRD profiles and by the AC susceptibility data was performed (see Table 1). All the MNPs were superparamagnetic at room temperature and the estimation of τ_N from AC data using the phenomenological Vogel – Fulcher eq. (4), reported in Table 1, showed a good agreement with the corresponding NMR data. This correspondence of values obtained from a sample-averaged technique, namely AC susceptibility, and a strongly local technique, namely NMR, is worth to be noted. The above mentioned dependence of the fitting parameters P and Q on magnetic anisotropy and particle size is largely confirmed by the trend of P/Q ratio as a function of the size and composition of the magnetic core, as can be seen in Table 1.

Table 1. Fitting parameters

Sample	τ_N (s rad ⁻¹) AC	τ_N (s rad ⁻¹) NMR	d (nm) TEM	P/Q
S-Mag/W-1	$5.34 \pm 1.00 \times 10^{-9}$	$9.73 \pm 5.51 \times 10^{-10}$	4.1 ± 0.6	0.45 ± 0.19

S-Mag/W-2	$2.80 \pm 0.67 \times 10^{-10}$	$2.82 \pm 1.66 \times 10^{-9}$	6.7 ± 0.8	0.00
S-Mag/W-3	$4.40 \pm 0.52 \times 10^{-7}$	$9.58 \pm 2.80 \times 10^{-8}$	18.2 ± 1.1	0.06 ± 0.02
P-Mag/W-1	-	$2.71 \pm 2.94 \times 10^{-9}$	5.5 ± 0.6	0.46 ± 0.29
P-Mag/W-2	-	$2.17 \pm 1.81 \times 10^{-9}$	8.0 ± 0.8	0.00 ± 0.11
P-Mag/W-3	$1.19 \pm 0.22 \times 10^{-8}$	$3.36 \pm 1.36 \times 10^{-9}$	12.0 ± 0.7	0.06 ± 0.11
P-Mag/T-1	$3.44 \pm 0.45 \times 10^{-14}$	$1.39 \pm 1.12 \times 10^{-9}$	5.5 ± 0.6	0.32 ± 0.26
P-Mag/T-2	$3.78 \pm 0.12 \times 10^{-9}$	$3.30 \pm 1.68 \times 10^{-9}$	8.0 ± 0.8	0.06 ± 0.06
P-Mag/T-3	$4.29 \pm 0.52 \times 10^{-9}$	$2.02 \pm 2.07 \times 10^{-9}$	12.0 ± 0.7	0.00
MnFe/T-1	$1.34 \pm 0.10 \times 10^{-12}$	$3.33 \pm 1.01 \times 10^{-10}$	3.0 ± 0.2	1.06 ± 0.31
MnFe/T-2	-	$7.13 \pm 3.81 \times 10^{-10}$	4.8 ± 0.1	0.49 ± 0.12
MnFe/T-3	$1.36 \pm 0.17 \times 10^{-9}$	$1.63 \pm 3.03 \times 10^{-10}$	6.0 ± 0.2	0.80 ± 0.30
CoFe/T-1	-	$2.89 \pm 2.33 \times 10^{-7}$	8.6 ± 1.1	0.08 ± 0.09
CoFe/T-2	$4.32 \pm 0.31 \times 10^{-5}$	$5.21 \pm 3.38 \times 10^{-6}$	8.6 ± 1.1	0.06 ± 0.13
CoFe/T-3	$3.11 \pm 0.31 \times 10^{-9}$	$6.24 \pm 2.54 \times 10^{-9}$	6.0 ± 1.4	0.05 ± 0.09
CoFe/T-4	$3.31 \pm 0.53 \times 10^{-9}$	$2.05 \pm 1.85 \times 10^{-9}$	5.0 ± 1.2	0.05 ± 0.15

From left to right: Estimation of Néel relaxation time by AC and NMR data, nanoparticles size by TEM measurements and P/Q ratios. Reported AC τ_N are estimated by fitting the AC susceptibility data to Vogel Fulcher equation (4). NMR τ_N and P/Q are obtained by the analysis of ¹H - NMRD profiles employing Roch's model. The studied nanoparticles were: rhamnose-coated magnetite NPs (S - Mag), oleate coated magnetite particles (P - Mag), oleic acid-coated manganese ferrite nanocrystals (MnFe) and non-stoichiometric oleic acid - coated cobalt ferrite (Co_xFe_{3-x}O₄) NPs (CoFe). Label T denotes samples dispersed in Toluene, label W samples dispersed in water solutions.

In 62 we studied maghemite superparamagnetic MNPs coated by PolyAcrylic Acid (PAA) and with different core sizes by means of longitudinal nuclear r_1 profiles and transversal nuclear r_2 profiles. This was one of the few cases^{53, 64, 65, 67, 73} where it was possible to measure r_2 values at ν less than few MHz, paying attention to the experimental parameters of the measurements, given the peculiarities of Fast Field Cycling (FFC) technology necessary to reach low frequencies: the instability of the acquisition field and the need of refocusing pulses during the FFC relaxation period. MNPs studied in 62 were specifically designed with the same PAA coating and three different sizes of the magnetic core ($d = 10, 14$ and 19 nm) in order to tailor their physical properties. The experimental longitudinal relaxivities profiles (see Figure 2) for MNPs of 10 and 14 nm showed a flattening of r_1 at low ν and a maximum at ν of few MHz with a subsequent drop for $\nu \geq 10$ -20 MHz. The sample with 19 nm magnetic core showed a strongly enhanced r_1 and this relatively high core size causes the flattening of the maximum at intermediate frequencies. On the other hand, the r_1 profile of 19 nm MNPs showed



a higher contrast efficiency compared to the other two samples, which behaved substantially in the same way.

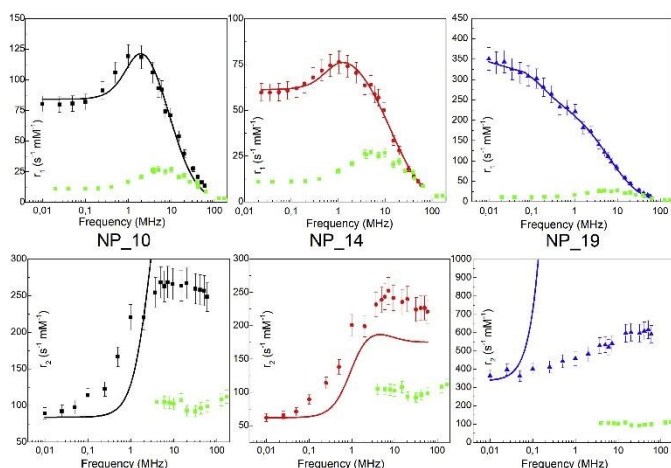


Figure 2. Longitudinal r_1 (upper) and transverse r_2 (bottom) NMRD profiles of the MNPs in ref. 54 collected at room temperature in the frequency range $0.01 < \nu < 60$ MHz and the best - fit curves obtained by applying the Roch's model (solid lines). r_1 and r_2 profiles of the (dismissed) commercial compound Endorem[®] are reported as green symbols in all graphs.⁶² Reprinted with permission from ref. [“Tailoring the magnetic core of organic-coated iron oxides nanoparticles to influence their contrast efficiency for Magnetic Resonance Imaging”, Basini M., Guerrini A., Cobianchi M., Orsini F., Bettiga D., Avolio M., Innocenti C., Sangregorio C., Lascialfari A., Arosio P., *Journal of Alloys and Compounds*, 770 (2019), 58, doi: doi.org/10.1016/j.jallcom.2018.08.120]. Copyright 2019, Elsevier.

The fitting procedure by Roch model well reproduced r_1 experimental curves providing τ_N in accordance with the core size: upon increasing the particle size, the spin dynamics slow down till spin freezing at low frequencies for 19 nm MNPs (NP_19). At the same time, the extrapolated values of P and Q parameters were perfectly correlated to the obtained τ_N as core size passes from 10 nm to 19 nm, Q increases indicating a progressively higher magnetic anisotropy barrier of the system. Lastly, the r_d evaluated by NMR fitting were compared with TEM and AFM data and suggested an impermeability of the coating. The measured r_2 profiles were compared with the predicted r_2 NMRD profiles calculated with the parameters obtained from the r_1 fitting. In Figure 2, it is evident that the theoretical curve predicted for r_2 disagreed with the experimental data all over the frequency range measured.

The same conclusion was attained in 64 where the effect of size, shape and dispersant on the dynamical magnetic properties of colloidal suspensions of MNPs was investigated. In this study spherical nanoparticles with an average diameter of 3.5, 8.5 and 17.5 nm dispersed in hexane were measured with ¹H - NMR relaxometry and compared (see Figure 3(a)).

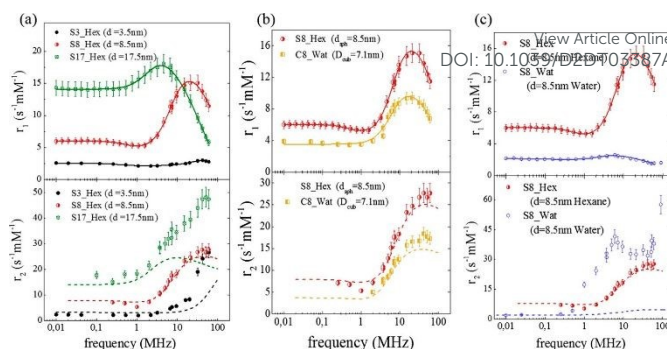


Figure 3. Longitudinal (r_1) and transverse (r_2) relaxivities (NMRD profiles) at room temperature measured on samples with different size (a), shape (b), and dispersant (c) in 64. The solid lines represent the best - fit curves of r_1 obtained from the Roch's model and the dashed lines are the r_2 curves calculated using Roch's model and the best fit parameters obtained for r_1 . Reproduced from ref. [“Local spin dynamics of iron oxide magnetic nanoparticles dispersed in different solvents with variable size and shape: A ¹H NMR study”, M. Basini, T. Orlando, P. Arosio, M. F. Casula, D. Espa, S. Murgia, C. Sangregorio, C. Innocenti, A. Lascialfari, *J. Chem. Phys.* 2017 (146), 034703; doi: 10.1063/1.4973979], with the permission of AIP Publishing.

Also, in this study r_1 NMRD profiles showed the typical behaviour of superparamagnetic MNPs and the NMR Néel relaxation time τ_N at room temperature ($\tau_N = 10^{-10} - 10^{-7}$ s), obtained using the Roch model, confirmed the results of DC and AC magnetic measurements. Again the trend followed by P and Q parameters was well correlated to the anisotropy energy barrier estimated by magnetic measurements, and to the slowing down of τ_N by increasing the superparamagnetic MNPs size, except for the 3.5 nm sample that exhibited quite long times for both NMR and magnetic measurements techniques. Unfortunately, also in 64 the r_2 curves calculated using r_1 fitting parameters did not reproduce the experimental profiles especially in the high field region. The results on the transversal nuclear relaxivity of the superparamagnetic MNPs were discussed using the universal scaling law proposed by Vuong et al.⁴⁸ for nanoparticles in the Motional Averaging Regime (MAR),⁷⁴ where the Redfield condition $\Delta\omega\tau_D < 1$ is fulfilled (τ_D being the diffusion time and $\Delta\omega$ the angular frequency shift experienced by a proton at the equator of the particle). Vuong et al. showed that, for external magnetic field > 1T, r_2 depends on the particle hydrodynamic diameter according to

$$\frac{r_2 \varphi_{intra}}{M_V^2} = a_{exp} d_H^2 = 11.6 \cdot 10^{-12} d_H^2 \quad (9)$$

where d_H is the particle hydrodynamic diameter, M_V the total magnetic moment divided by the particle volume and φ_{intra} the intra - aggregate volume fraction of cluster and hybrid magnetic materials. In the case of ref. 62, the experimental r_2 values at $\nu = 60$ MHz were very close to the ones predicted by the scaling law also for the 19 nm sample that felt outside of the MAR regime, while in the case of ref. 64, only the spherical sample of 8.5 nm did not follow the Vuong scaling law.

The influence of the chemical composition of magnetic core in MNPs on the relaxometric properties was studied in 63, where $Co_xZn_yFe_{3-(x+y)}O_4$ nanoparticles were investigated. In this study, the



Co content was maintained constant ($x = 0.6$), while a gradually substitution of iron by Zn^{2+} ($0 \leq y \leq 0.4$) allowed the study of the effect of zinc inclusion on the magnetic properties of MNPs. The longitudinal nuclear relaxivity profiles confirmed a clear decrease of the magnetic anisotropy upon Zn content increasing, as pointed out by the magnetic measurements. In the absence of Zn, r_1 showed the typical shape of a high magnetic anisotropy system, namely a plateau at low frequencies followed by a drop for $\nu \gtrsim$ few MHz, whereas r_1 for particle with the highest content of Zn ($y = 0.4$) presented a maximum at intermediate frequencies (at $\nu \sim 1.5$ MHz), preceded by a plateau at low frequencies and followed by a decrease at high frequencies, denoting a lower degree of magnetic anisotropy (see Figure 4). The fitting of r_1 NMRD profiles with the Roch model allowed again the estimation of the values of τ_N , r_d and M_s . Here below the ranges of values found in 55: $2.4 \times 10^{-8} \text{ s} < \tau_N < 3.2 \times 10^{-7} \text{ s}$, $5.6 \text{ nm} < r_d < 9.4 \text{ nm}$, $76 < M_s < 80 \text{ Am}^2/\text{kg}$. Transverse r_2 relaxivities were measured only for three magnetic fields, as reported in Figure 4 (b), and showed a marked dependence on the Zn content reaching 4 - 5 times higher values compared to Endorem® in the case of Zn content $y = 0.4$.

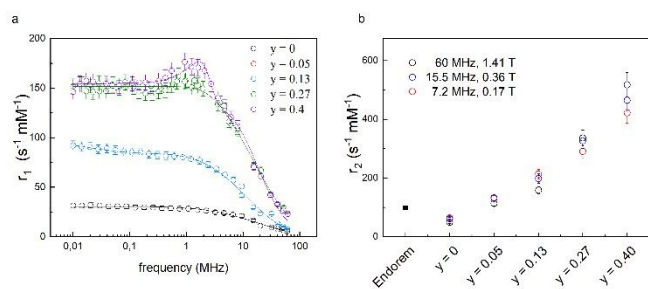


Figure 4. (a) Longitudinal r_1 relaxivity profiles and best-fit curves. (b) Transverse r_2 relaxivities values measured at 7.2, 15.5, and 60 MHz as a function of the Zn amount compared with dismissed commercial compound (Endorem®) (data acquired at 1.41 T) in 63. Reprinted with permission from ref. [“Role of Zn^{2+} Substitution on the Magnetic, Hyperthermic and Relaxometric Properties of Cobalt Ferrite Nanoparticles”, Albino M., Fantechi E., Innocenti C., López-Ortega A., Bonanni V., Campo G., Pineider F., Gurioli M., Arosio P., Orlando T., Bertoni G., de Julián Fernández C., Lascialfari A., Sangregorio C., *J. Phys. Chem. C*, 123 (2019), 6148; doi: 10.1021/acs.jpcc.8b10998]. Copyright 2019, ACS Publications.

3.3 The role of the shape

The effect of the MNPs' shape was studied in 64, where the 8.5 nm spherical sample of superparamagnetic MNPs was compared to an analogous cubic - shaped sample with square edge size of 7.1 nm and diagonal size of 8.1 nm, in order to have nanoparticles with comparable volume. The longitudinal relaxivity reported in Figure 3(b) shows lower values for the cubic - shaped sample over the whole frequency range. Both samples present similar superparamagnetic behaviour with small differences: the maximum of r_1 of the cubic sample is slightly shifted at lower frequency ($\nu = 15 - 20$ MHz) with respect to the maximum of the spherical sample ($\nu = 20 - 25$ MHz) and the dispersion at low field is less pronounced.

The fitting procedure of the cubic sample r_1 NMRD profile provided values of P/Q , τ_N and r_d parameters slightly different from the

spherical sample and this discrepancy can be easily justified by considering the results obtained by other techniques (magnetic measurements, TEM, etc.). The r_2 theoretical profile of samples obtained by using the best-fitting parameters evaluated for the corresponding r_1 does not reproduce adequately all the experimental curves, showing larger discrepancies at high fields for both samples and some failures around 1 MHz for the spherical one.

3.4 The influence of solvent

Another factor that can influence the superparamagnetic relaxation is the kind of solvent in which the MNPs are dispersed, as well as the correlated MNPs surface engineering necessary to allow their dispersion in water or in physiological solutions, a crucial condition for their potential application in biomedicine. In 61 and 64 we partially investigated the effect of different surface engineering on the spin dynamics. In 61, oleate coated magnetite particles dispersed in toluene (P - Mag/T series) and in water (P - Mag/W series) were compared. It was not easy to single out a clear picture of the consequences of using different dispersion solvents, also because the recorded effects are simultaneously related to the coating needed to effectively carry out the dispersion (see next section). Observing Figure 5, the r_1 - maxima of P - Mag/W - 1, P - Mag/W - 2 and the “corresponding” samples P - Mag/T - 1, P - Mag/T - 2 were shifted in frequency, while the maximum of P - Mag/W - 3 and P - Mag/T - 3 was un-shifted. Moreover, r_1 values differed slightly for the couples P - Mag/W - 1 || P - Mag/T - 1 and P - Mag/W - 3 || P - Mag/T - 3; on the contrary, they decreased passing from P - Mag/T - 2 to P - Mag/W - 2. At the same time, the P/Q results obtained from the fitting suggested that the contribution from the Curie relaxation mechanism was enhanced from toluene to water. The hypothesis proposed was that the surface coating of P - Mag/W - series, modified by using a poly(maleicanhydride) polymer shell intercalated with oleate molecules, produced an effect on the nuclear relaxometric properties by changing the distance of minimum approach of the solvent molecules.



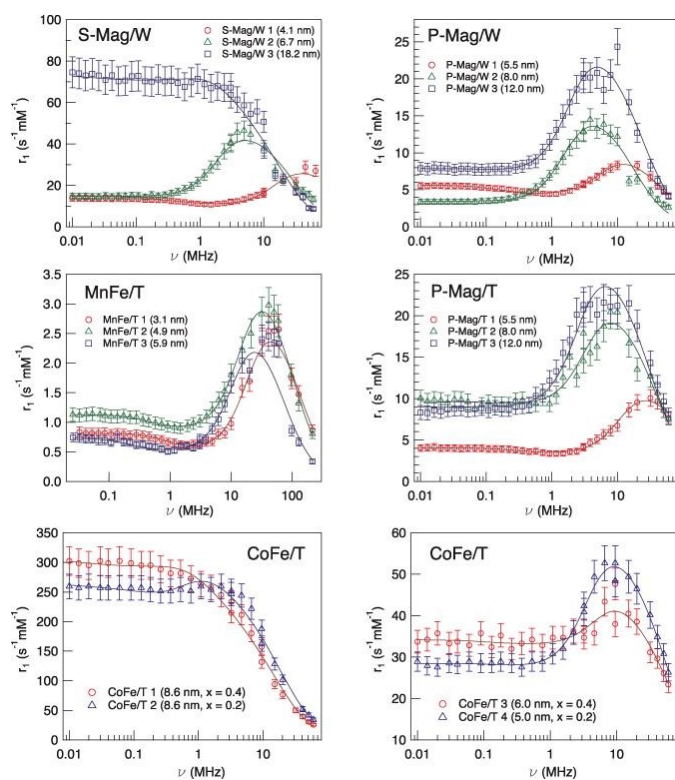


Figure 5. Longitudinal r_1 relaxivity profiles at room temperature and best-fit curves obtained with Roch's model (solid lines) for sample series S - Mag/W, P - Mag/T, P - Mag/W, MnFe/T and CoFe/T in 61. Reproduced with permission from ref. ["NMR-D study of the local spin dynamics and magnetic anisotropy in different nearly monodispersed ferrite nanoparticles", Bordonali L., Kalaivani T., Sabareesh K.P.V., Innocenti C., Fantechi E., Sangregorio C., Casula M.F., Lartigue L., Larionova J., Guari Y., Corti M., Arosio P., Lascialfari A., *Journal of Physics: Condensed Matter*, 25 (2013), 066008, doi: 10.1088/0953-8984/25/6/066008] © IOP Publishing. All rights reserved.

In 64 MNPs of 8.5nm were dispersed in aqueous based dispersant adding a ternary system made of monoolein, lauroylcholin, and water to compare the nuclear relaxivity performances with a sample with the same magnetic core dispersed in hexane. The first evidence was a drastic lowering of r_1 in the whole frequency range and the shift of the maximum position to lower magnetic fields for the sample dispersed in water in comparison with the one in hexane (see Figure 3 (c)). At the same time, for the water dispersed sample the value of τ_N obtained by fitting of NMR profiles was one order of magnitude higher than the τ_N of the sample in hexane, reflecting an enhancement of magnetic anisotropy energy barrier as resulting from AC measurements. In addition, the distance of minimum approach between the protons of the solution and the superparamagnetic MNPs centre was clearly increased when they are dispersed in water. The influence of the solvent on nuclear relaxation time T_2 appeared dramatically evident since the transfer into a water-based dispersant increased r_2 values of the superparamagnetic MNPs on all the range of investigated fields, the reproducibility of which was completely failed when r_2 curve calculated with the fitting parameters of r_1 are used. A partial explanation of this behaviour could be ascribed to the particle

aggregation due to the dispersant effect for water-based sample, as explained in ref. 64, that prevents the diffusion of solvent near the magnetic centre (T_1 effect), but, at the same time, makes nuclear spin-spin hyperfine interactions more efficient (T_2 effect).

3.5 The effect of coating

In order to study the coating effect on the relaxometric properties of MNPs, we recently investigated two series of nanoparticles composed of a maghemite core with mean diameters $d = 17$ and 8 nm coated with four different negative polyelectrolytes. The magnetic measurements indicated that both MNPs can be considered superparamagnetic at room temperature, because, even for the larger sample, the average blocking temperature is lower than 300 K. The experimental longitudinal relaxivity profiles of 17 nm superparamagnetic MNPs showed a constant increase of r_1 with lowering the external magnetic fields, without the expected plateau at low fields, while a typical superparamagnetic trend of r_1 profiles for the 8 nm samples, i.e. the presence of a maximum of the relaxivities and a slight dispersion at low fields, was found. The transverse relaxivity profiles of the 8 nm samples were similar to the one of the commercial Endorem® both as concerns values and frequency behaviour, whereas in the case of the 17 nm sample the r_2 curves denoted a markedly increased relaxation efficiency. It is worth noting that the 17 nm sample coated with a copolymer of poly(methacrylic acid) (PMAA) with polyethylene glycol (PEG) displayed r_2 values smaller than those of all the other samples at high Larmor frequencies. This result can be tentatively justified by a different surface spin disorder and/or particle aggregation effects induced by the PMAA - PEG copolymer. For what concerns the fitting of the 17nm sample curves, we were not able to apply the Roch model probably because of the quite broad size distribution that didn't comply with the limit of validity of the model (i.e. MNPs diameter < 20 nm). On the contrary, we were able to fit r_1 profiles of the 8 nm superparamagnetic MNPs obtaining Néel relaxation times values typical for superparamagnetic nanoparticles of this size ($3.5 \cdot 10^{-9} \text{ s} < \tau_N < 3.9 \cdot 10^{-9} \text{ s}$) and a distance of minimum approach of $1 \div 2$ nm greater than the estimated core radius, thus proving water molecules inability to diffuse completely inside the coating.

3.6 The effect of functionalization

As a further factor that could influence the nuclear relaxation mechanisms, we briefly investigated the effects of MNPs functionalization on the relaxivity. In details, with the purpose to design a theranostic agent, in 66 a biocompatible nanocarrier was decorated with folate for targeting human breast MDA - MB - 231 tumor and loaded with magnetite nanoparticles and the antitumoral drug Paclitaxel (PTX). The functionalization effect was particularly evident on the transversal relaxivity. Indeed, the r_2 values doubled in the Larmor frequency range investigated ($7 < \nu < 60 \text{ MHz}$) when the organic carrier + magnetite core was functionalized with folate or with folate plus PTX, reaching r_2 values up to 8 times higher with respect to Endorem®. These surprising results were confirmed by *in vivo* MRI experiments on nude mice that showed how the developed



nanocarrier acted as negative CA with better performances than Endorem® and was able to target MDA - MB - 321 cells residing in the tumor area for long time, up to some days.

In 67 we exploited the conjugation between Peptide Nucleic Acid (PNA) oligomers and superparamagnetic MNPs in order to improve the PNA solubility and their cell permeability, being these oligomers interesting for gene therapy applications. As showed by the ¹H-NMR results reported in 67, the MNPs shortened the longitudinal and transverse nuclear relaxation times, enhancing the correlated relaxivities. This effect resulted less marked in the case of functionalized nanoparticles if compared to un-functionalized ones for r_1 , while in the case of r_2 a lower efficiency in shortening the transverse relaxation time was registered for functionalized MNPs for Larmor frequency below 0.2 MHz. The differences in relaxivity values, between the MNPs PNA functionalized or not, could be justified by the increased size of particles once functionalized, as showed by AFM measurements, as well as by the poor solubility of PNA. After MNP functionalization, the water molecules encountered more obstacles to approach the magnetic cores of nanoparticles, thus decreasing the efficacy in shortening the nuclear relaxation times.

4. Discussion

The aforementioned studies 61 - 67 allow us to discuss the results according to the microscopic characteristics of each kind of iron-oxide nanoparticles investigated. The strong dependence of nuclear relaxation properties on the size and composition of the magnetic core was confirmed by the experimental NMRD profiles. Indeed, the crystallinity, the magnetic anisotropy and the volume of the superparamagnetic MNPs influence directly their saturation magnetization and some correlation times, e. g. the rotational (τ_R), electronic relaxation (τ_N) and diffusion (τ_D) times. On the other hand, the shape of superparamagnetic MNPs seems to be less effective in perturbing the nuclear relaxation time of protons of the host media, see 64.

The influence of the solvent on the relaxometric properties of MNPs deserves a separate discussion. In fact, this effect cannot be separated by the coating procedure implemented in the synthetic protocols and a generalization of the influence of such synthetic process on the r_1 and/or r_2 behaviour is still difficult to be evinced. The role of the solvent depends on which coating is used to cover the magnetic core but also on the synthetic path used to pass from hydrophobic conditions (normally the MNPs are first synthesized in organic solvents) to hydrophilic ones (e.g. exchanging of organic capping agents by polymers, acids, etc. or using amphiphilic coating that intercalates with aliphatic domains, or other choices). For a so complex situation, although effects on the MNPs relaxation properties are thoroughly expected, the possible causes are really difficult to be evinced, as seen in the example reported in 61, where similar systems differing only in size (P-Mag/ series) behaved in a different manner.

Another noteworthy aspect is the impact of the type of coating on relaxivity. Indeed, it should be important to understand if the coating

is only an inert "spacer" between the magnetic core and the protons of the solvent or it is involved in the nuclear spin dynamics. In this perspective, we reported results in 65 that showed how different coatings on superparamagnetic MNPs similar in size didn't influence the relaxivity profiles. At the same time, some of us recently demonstrated by means of low - field muon spin relaxation measurements⁷⁵ on full or hollow core maghemite superparamagnetic MNPs how it is crucial to study high surface/volume ratio MNPs to unravel the influence of surface spin effects on spin dynamics. Indeed, since the coating can modify the magnetic order of the surface spins for chemical-physical reasons, we think that it could be important to systematically study small MNPs (at fixed core size below 4 - 6 nm) with different coatings using NMR with the purpose to single out their role in nuclear relaxation mechanisms and related spin surface effects.

Finally, for the effect of coating functionalization, as in the case of solvent effects, a large number of cases of MNPs with the same core but different coating/functionalization are needed. Once again, the functionalization influences both r_1 and r_2 and its effect strongly depends on which type of chemical moiety (molecules, oligomers, antigen, antibody, etc...) is used.

As a last observation, it is worth reminding that the possibility to use theoretical models to interpret the longitudinal relaxivity experimental curves (Roch model in our papers) allowed us to extrapolate important quantitative information on the physical properties of the investigated superparamagnetic MNPs, like the distance of minimum approach of solvent protons to nanoparticles or the Neel relaxation time. In all the studied superparamagnetic MNPs, r_1 experimental data are well fitted by the heuristic theoretical model, and the parameters obtained clarify the nuclear spin mechanisms involved in the spin-lattice relaxation for all the nanoparticles that fulfilled MAR regime. On the other hand, if the parameters obtained by the r_1 fitting procedure are used also for predicting r_2 profiles, the model does not properly describe all the experimental data. This point strongly suggests that physical mechanisms, not included in Roch's model, can contribute to the nuclear spin-spin relaxation. Currently, there is no clear indication on which mechanisms can be invoked to improve the model, possible ones being the electronic dipole - dipole interactions between the single MNPs, a magnetic anisotropy other than uniaxial, the Brownian spin dynamics, the contribution from the water chemical exchange (if any) and the surface spins dynamics.

In order to summarize the effect of different intrinsic parameters of MNPs on their relaxometric properties, we reported in Table 2 a level of influence of each parameter on relaxivities that could be used as a recommendation guide for the researchers.



Table 2. Influence of intrinsic parameters

Intrinsic parameters	Influence on relaxivities	Comments
Core dimension	****	Optimal range 11-20nm
Core composition	****	Limited by toxicity
Solvent type	***	Correlated to type of coating
Shape	*/**	-
Coating	**	More evident for small MNPs (below 4-5 nm)
Coating functionalization	**/**	Strongly dependent on chemical moiety used

From left to right: List of MNPs intrinsic parameters, level of influence on relaxivities (* low, ** medium-low, *** medium-high, **** high) and general comments.

5. Conclusions

In this perspective, we present and discuss our research activity of last 10 years focused on the comprehension of the physical mechanisms at the basis of the nuclear relaxation of superparamagnetic nanoparticles as a function of their chemical-physical properties.

Summarizing, the overall results showed a clear dependence of nuclear relaxivities r_1 and r_2 on the composition and size of superparamagnetic MNPs magnetic core and the solvent used to disperse superparamagnetic MNPs. In the case of maghemite/magnetite MNPs, which remain the most used up to now for their low toxicity, the diameter of the magnetic core should be preferably bigger than 11-12 nm for obtaining a sizeable effect on the relaxometric efficiency, at least comparable to ENDOREM. Doping iron oxides MNPs with Co, Mn, Zn, etc. strongly influences the nuclear relaxivities and their dependence on field intensity, often leading to better results if compared with undoped MNPs. At the same time, these kinds of ions, if released in the cells, impact on the biocompatibility of the MNPs due to their toxicity and thus imply extensive studies on their cytotoxicity.

The effects of shape, coating and functionalization of the superparamagnetic MNPs need to be further investigated and interpreted also in view of developing effective models to predict their efficiency as MRI contrast agents.

Nevertheless, we recommend to the research community involved in the MNPs synthesis and characterization an effort in the direction of investigating new systems where microscopic characteristics, like shape and coating, are changed in a systematic way. No clear and undisputed recommendation about the best features of shape and coating can be provided till now, mainly because of the absence of just mentioned systematic investigation. In fact, we observe that only by studying the magnetic behaviour as a function of one MNP parameter fixing the others (e.g. varying the shape and fixing the coating, composition, size, solvent, etc.), the obtained experimental results could be rationalized. For example, the

great variability of type of functionalization from one group to another, makes the interpretation of the results very complex and not unique. In order to reach this goal, a large number of MNPs should be available to the researchers.

As concerns the data interpretation, we adopted the heuristic model of Roch *et al.* to interpret our experimental NMR-D profiles and describe the spin dynamics involved in the relaxation processes quantifying its effects. The application of the model to a large number of cases pointed out a clear difference between its ability to describe longitudinal and transverse relaxivity. In the first case, indeed, the model was able to satisfactorily fit r_1 profiles of many different superparamagnetic MNPs providing information on some of their physical quantities such as, for instance, the Néel correlation time τ_N , felt by NMR and the distance of minimum approach r_d of solvent molecules near the superparamagnetic MNPs. As the r_2 profiles are not well reproduced, we wish that this perspective could be a stimulus for future developments of theoretical models capable to describe more extensively the nuclear magnetic relaxation of this type of nanoparticles.

Author Contributions

The manuscript was written, reviewed and edited through contributions of all authors. All authors have given approval to the final version of the manuscript.

Conflicts of interest

There are no conflicts to declare.

Acknowledgements

EU COST project Eurelax (CA15209) is gratefully acknowledged. P.A. thanks Dipartimento di Fisica, Università degli Studi di Milano (Italy), for its support. INFN (National Institute for Nuclear Physics) is also acknowledged for the support provided via PROTHYP and NAMASSTE projects.

References

- 1 L.-M. Lacroix, D. Ho, S. Sun, *Curr. Top. Med. Chem.*, 2010, **10**, 1184–97.
- 2 A.K.A. Silva, A. Espinosa, J. Kolosnjaj-Tabi, C. Wilhelm, F. Gazeau, *Iron Oxides: From Nature to Applications*, 2016, Editor: D. Faivre, Wiley VCH, 425–471.
- 3 L. Yang, Z. Zhou, J. Song, X. Chen, *Chemical Society reviews*, 2019, **48**, 5140–5176.
- 4 S. Laurent, D. Forge, M. Port, A. Roch, C. Robic, L. Vander Elst, R.N. Muller, *Chem. Rev.*, 2008, **108**, 2064–2110.
- 5 S. Bajpai, S. Kr Tiwary, M. Sonker, A. Joshi, V. Gupta, Y. Kumar, N. Shreyash, S. Biswas, *ACS Appl. Nano Mater.*, 2021, **4**, 6441–6470.
- 6 F. Yan, Y. Wang, S. He, S. Ku, W. Gu, L. Ye, *J. Mater. Sci. Mater. Med.*, 2013, **24**, 2371e2379.
- 7 T. Sun, Y. Liu, C. Zhou, L. Zhang, X. Kang, S. Xiao, Me. Du, Z. Xu, Y. Liu, G. Liu, M. Gong, D. Zhang, *Nanoscale*, 2021, **13**, 7638.



- 8 J. Song, L. Lin, Z. Yang, R. Zhu, Z. Zhou, Z.W. Li, F. Wang, J. Chen, H. Yang, X. Chen, *J. Am. Chem. Soc.*, 2019, **141**, 8158–8170
- 9 Z. Shen, W. Fan, Z. Yang, Y. Liu, V.I. Bregadze, S.K. Mandal, B.C. Yung, L. Lin, T. Liu, W. Tang, L. Shan, Y. Liu, S. Zhu, S. Wang, W. Yang, L.H. Bryant, D.T. Nguyen, A. Wu, X. Chen, *Small* 2019, **15**, 1903422.
- 10 X.R. Song, S.H. Li, J. Dai, L. Song, G. Huang, R. Lin, J. Li, G. Liu, H.H. Yang, *Small*, 2017, **13**, 1603997.
- 11 Li-Sen Lin, Xiangyu Yang, Zijian Zhou, Zhen Yang, Orit Jacobson, Yijing Liu, Angela Yang, Gang Niu, Jibin Song,* Huang-Hao Yang,* and Xiaoyuan Chen, *Advanced Materials*, 2017, **29**, 1606681.
- 12 D.-E. Lee, H. Koo, I.-C. Sun, J.H. Ryu, K. Kim, I.C. Kwon, *Chem. Soc. Rev.*, 2012, **41**, 2656–72.
- 13 R. Di Corato, F. Gazeau, C. Le Visage, D. Fayol, P. Levitz, F. Lux, D. Letourneur, N. Luciani, O. Tillement, C. Wilhelm, *ACS Nano*, 2013, **7**, 7500–7512.
- 14 J.L. Bridot, A.C. Faure, S. Laurent, C. Rivière, C. Billotey, B. Hiba, M. Janier, V. Jossrand, J.L. Coll, L. Vander Elst, R. Muller, S. Roux, P. Perriat, O. Tillement, *J. Am. Chem. Soc.*, 2007, **129**, 5076–5084.
- 15 C. Tassa, S.Y. Shaw, R. Weissleder, *Accounts Chem. Res.*, 2011, **44**, 842–852.
- 16 Qin, Zhiguo; Chen, Bo; Mao, Yu; Shi, Chu; Li, Yan; Huang, Xiao; Yang, Fang; Gu, Ning, *ACS App. Mat. Interf.* 2020, **12**, 57382–57390.
- 17 X. Guan, J. Li, J. Cai, S. Huang, H. Liu, S. Wang, X. Zhang, Y. Sun, H. Liu, G. Xie, Z. Wang, *Chemical Engineering Journal*, 2021, **425**, 130579.
- 18 Q. Liu, L. Liu, C. Mo, X. Zhou, D. Chen, Y. He, H. He, W. Kang, Y. Zhao, G. Jin, *Journal of Nanobiotechnology*, 2021, **19**, 171.
- 19 R. Hergt, S. Dutz, R. Müller, M. Zeisberger, *J. Phys.: Condens. Matter*, 2006, **18**, S2919.
- 20 S. Dutz, R. Hergt, *Nanotechnology*, 2014, **25**, 452001.
- 21 S. Dutz, N. Buske, J. Landers, C. Gräfe, H. Wende, J.H. Clement, *Nanomaterials* 2020, **10**, 1019.
- 22 P. Pradhan, J. Giri, G. Samanta, H.D. Sarma, K.P. Mishra, J. Bellare, R. Banerjee, D. Bahadur, *J. Biomed. Mater. Res. Part B Appl. Biomater.*, 2006, **81B**, 12e22.
- 23 D. Cabrera, J. Camarero, D. Ortega, F.J. Teran, *J. Nanopart. Res.*, 2015, **17**, 121.
- 24 W. Wang, F. Li, S. Li, Y. Hu, M. Xu, Y. Zhang, M.I. Khan, S. Wang, M. Wu, W. Ding, B. Qiu, *Journal of Materials Science and Technology*, 2021, **81**, 77 – 87.
- 25 N. Shreyash, M. Sonker, S. Bajpai, S. Kr Tiwary, *ACS Appl. Bio Mater.*, 2021, **4**, 2307–2334.
- 26 M. Arruebo, R. Fernández-Pacheco, M. Ricardo Ibarra, J. Santamaría, *Nano Today*, 2007, **2**, 22–32.
- 27 A.P. Douvalis, R. Zboril, A.B. Bourlinos, J. Tucek, S. Spyridi, T. Bakas, *J. Nanopart. Res.*, 2012, **14**, 1130.
- 28 B. Chertok, B.A. Moffat, A.E. David, F. Yu, C. Bergemann, B.D. Ross, V.C. Yang, *Biomaterials*, 2008, **29**, 487e496.
- 29 C.S.S.R. Kumar, F. Mohammad, *Adv. Drug Deliv. Rev.*, 2011, **63**, 789e808.
- 30 S.W. Lee, S.H. Lee, S. Biswal, *Theranostics*, 2012, **2**, 403e412.
- 31 K. Wu, D. Su, J. Liu, R. Saha, J.-P. Wang, *Nanotechnology*, 2019, **30**, 502003.
- 32 G. Schmid, *Nanoparticles: From Theory to Application*, Wiley-VCH, Weinheim, 2004.
- 33 K. J. Klabunde, *Nanoscale Materials in Chemistry*, Wiley-Intersc., New York, 2001.
- 34 A. P. Alivisatos, *Science*, 1996, **271**, 933.
- 35 M. P. Pileni, *Nat. Mater.*, 2003, **2**, 145.
- 36 V.K. Varadan, L.F. Chen, J. Xie, *Nanomedicine: Design and Applications of Magnetic Nanomaterials, Nanosensors and Nanosystems*, Wiley, 2008.
- 37 H. Rui, R. Xing, Z. Xu, Y. Hou, S. Goo, S. Sun, *Adv. Mater.*, 2010, **22**, 2729e2742. View Article Online
DOI: 10.1039/D2DT03387A
- 38 A. Plan Sangnier, A.B. Van de Walle, A. Curcio, R. Le Borgne, L. Motte, Y. Lalatonne, C. Wilhelm, *Nanoscale*, 2019, **11**, 16488–16498.
- 39 E. Blanco, H. Shen, M. Ferrari, *Nat. Biotechnol.*, 2015, **33**, 941–951.
- 40 H. Shaghholani, S.M. Ghoreishi, S.H. Sharifi, *J. Drug Deliv. Sci. Technol.*, 2018, **45**, 373–377.
- 41 M. Mahmoudi, S. Laurent, M.A. Shokrgozar, M. Hosseinkhani, *ACS Nano*, 2011, **5**, 7263–7276.
- 42 P.M.L. Mojica, Jr.E. Lima, M.M. Vasquez, V.E. Tognoli, H.E. Troiani, A.A. Pasa, T.B. Creczynski-Pasa, A.H. Silva, P. Gurman, L. Colombo, G.F. Goya, *J. Biomed. Mater.*, 2014, **102**, 860–868.
- 43 F. Brero, M. Albino, A. Antocchia, P. Arosio, M. Avolio, F. Berardinelli, D. Bettega, P. Calzolari, M. Ciocca, M. Corti, A. Facchetti, S. Gallo, F. Groppi, A. Guerrini, C. Innocenti, C. Lenardi, S. Locarno, S. Manenti, R. Marchesini, M. Mariani, F. Orsini, E. Pignoli, C. Sangregorio, I. Veronese, A. Lascialfari, *Nanomaterials*, 2020, **10**, 1919.
- 44 R.S. Pereira, F.S. Prato, FCCPM, G. Wisenberg, J. Sykes, *Magnetic resonance in medicine*, 1996, **36**, 684–693.
- 45 M. Saeed, M.F. Wendland, Y. Takehara, T. Masui, C.B. Higgins, *Radiology*, 1992, **182**, 675–683.
- 46 C.L. Wolfe, M.E. Moseley, M.G. Wikstrom, R.E. Sievers, M.F. Wendland, J.W. Dupon, W.E. Finkbeiner, M.J. Lipton, W.W. Parmley, R.C. Brasch, *Circulation*, 1989, **80**, 969–982.
- 47 D. Kruk, A. Korpała, S. Mehdizadeh Taheri, A. Kozłowski, S. Förster, E. A. Rössler, *J. Chem. Phys.*, 2014, **140**, 174504.
- 48 Vuong Q.L., Berret JF., Fresnais J., Gossuin Y., Sandre O., *Adv. Healthcare Mater.*, 2012, **1**, 502–512.
- 49 M. Jeon, M.V. Halbert, Z.R. Stephen, M. Zhang, *Adv. Mater.* 2020, **33**, 1906539.
- 50 L. Yang, Z. Wang, L. Ma, A. Li, J. Xin, R. Wei, H. Lin, R. Wang, Z. Chen, J. Gao, *ACS Nano*, 2018, **12**, 4605–4614.
- 51 D. Bonvin, D.T. L. Alexander, A. Millán, R. Piñol, B. Sanz, G.F. Goya, A. Martínez, J.A.M. Bastiaansen, M. Stuber, K.J. Schenk, H. Hofmann, M.M. Ebersold, *Nanomaterials*, 2017, **7**, 225.
- 52 T. Vangijzegem, D. Stanicki, A. Panepinto, V. Socoliuc, L. Vekas, R.N. Muller, S. Laurent, *Nanomaterials*, 2020, **10**, 757.
- 53 Y. Gossuin, T. Orlando, M. Basini, D. Henrard, A. Lascialfari, C. Mattea, S. Stapf, Q.L. Vuong, *Nanotechnology*, 2016, **27**, 155706.
- 54 C. Blanco-Andujar, A. Walter, G. Cotin, C. Bordeianu, D. Mertz, D. Felder-Flesch, S. Begin-Colin, *Nanomedicine*, 2016, **11**, 1889–1910.
- 55 K.E. Kellar, D.K. Fujii, W.H.H. Gunther, K. Briley-Sabø, A. Bjornerod, M. Spiller, S.H. Koenig, *Academic Radiology*, 2002, **9**, S34–S37.
- 56 S. Laurent, A. Ouakssim, C. Nicotra, Y. Gossuin, A. Roch, L. Vander Elst, M. Cornant, P. Soleil, R.N. Muller, *Physica Status Solidi*, 2004, **1**, 3644–3650.
- 57 S.L.C. Pinho, S. Laurent, J. Rocha, A. Roch, M.-H. Delville, S. Mornet, L.D. Carlos, L. Vander Elst, R.N. Muller, C.F.G.C. Geraldes, *The Journal of Physical Chemistry C*, 2012, **116**, 2285–2291.
- 58 M. Levy, F. Gazeau, C. Wilhelm, S. Neveu, M. Devaud, P. Levitz, *J. Phys. Chem. C*, 2013, **117**, 15369–15374.
- 59 Q. L. Vuong, P. Gillis, A. Roch, Y. Gossuin, *Wiley Interdiscip. Rev.: Nanomed. Nanobiotechnol.* 2017, **9**, e1468.
- 60 A. Roch, R.N. Muller, P. Gillis, *J. Chem. Phys.*, 1999, **110**, 5403.
- 61 L. Bordonali, T. Kalaivani, K.P.V. Sabareesh, C. Innocenti, E. Fantechi, C. Sangregorio, M.F. Casula, L. Lartigue, J. Larionova, Y. Guari, M. Corti, P. Arosio, A. Lascialfari, *J. Phys.: Condens. Matter*, 2013, **25**, 066008.



Perspective

Dalton Transactions

- 62 M. Basini, A. Guerrini, M. Cobianchi, F. Orsini, D. Bettega, M. Avolio, C. Innocenti, C. Sangregorio, A. Lascialfari, P. Arosio, *J. Alloys and Compounds*, 2019, **770**, 58-66.
- 63 M. Albino, E. Fantechi, C. Innocenti, A. Lopez-Ortega, V. Bonanni, G. Campo, F. Pineider, M. Gurioli, P. Arosio, T. Orlando, G. Bertoni, C. de Julian Fernandez, A. Lascialfari, C. Sangregorio, *J. Phys. Chem. C*, 2019, **123**, 6148-6157.
- 64 M. Basini, T. Orlando, P. Arosio, M. F. Casula, D. Espa, S. Murgia, C. Sangregorio, C. Innocenti, A. Lascialfari, *J. Chem. Phys.*, 2017, **146**, 034703.
- 65 F. Brero, M. Basini, M. Avolio, F. Orsini, P. Arosio, C. Sangregorio, C. Innocenti, A. Guerrini, J. Boucard, E. Ishow, M. Lecouvey, J. Fresnais, L. Lartigue, A. Lascialfari, *Nanomaterials*, 2020, **10**, 1660.
- 66 P. Arosio, F. Orsini, A.M. Piras, S. Sandreschi, F. Chiellini, M. Corti, M. Masa, M. Múčková, L. Schmidtová, C. Ravagli, G. Baldi, E. Nicolato, G. Conti, P. Marzola, A. Lascialfari, *RSC Adv.*, 2015, **5**, 39760.
- 67 M. Galli, A. Guerrini, S. Cauteruccio, P. Thakare, D. Dova, F. Orsini, P. Arosio, C. Carrara, C. Sangregorio, A. Lascialfari, D. Maggioni, E. Licandro, *RSC Adv.*, 2017, **7**, 15500.
- 68 A. Roch, R.N. Muller, Longitudinal relaxation of water protons in colloidal suspensions of superparamagnetic crystal. *Proceedings of the 11th Annual Meeting of the Society of Magnetic Resonance in Medicine, Works in Progress* 1992, 1447.
- 69 S.H. Koenig, K.E. Kellar, *Magn. Reson. Med.*, 1995, **34**, 227.
- 70 A. Roch, R.N. Muller, P. Gillis, *J. Magn. Reson. Imaging*, 2001, **14**, 94.
- 71 L. Néel, *Ann. Géophys.* 1949, **5**, 99.
- 72 H. Vogel, *Phys. Z.*, 1921, **22**, 645; G. S. Fulcher, *J. Am. Ceram. Soc.*, 1925, **8**, 339.
- 73 P. Arosio, J. Thévenot, T. Orlando, F. Orsini, M. Corti, M. Mariani, L. Bordonali, C. Innocenti, C. Sangregorio, H. Oliveira, S. Lecommandoux, A. Lascialfari, O. Sandre, *J. Mater. Chem. B*, 2013, **1**, 5317.
- 74 Brooks R.A., Moyné F., Gills P., *Magn. Reson. Med.*, 2001, **45**, 1014-1020.
- 75 M. Basini, S. Sanna, T. Orlando, L. Bordonali, M. Cobianchi, P. Arosio, M. Mariani, D. Peddis, V. Bonanni, R. Mathieu, T. Kalaivani, G. Singh, J. Larionova, Y. Guari, L. Lartigue, A. Lascialfari, *Phys. Rev. B*, 2020, **102**, 195424.

View Article Online
DOI: 10.1039/D2DT03387A

Open Access Article. Published on 20 February 2023. Downloaded on 2/20/2023 3:53:54 PM.
This article is licensed under a Creative Commons Attribution-NonCommercial 3.0 Unported Licence.



Dalton Transactions Accepted Manuscript